Whole-animal functional and developmental imaging with isotropic spatial resolution

Raghav K Chhetri, Fernando Amat, Yinan Wan, Burkhard Höckendorf, William C Lemon & Philipp J Keller

Imaging fast cellular dynamics across large specimens requires high resolution in all dimensions, high imaging speeds, good physical coverage and low photo-damage. To meet these requirements, we developed isotropic multiview (IsoView) light-sheet microscopy, which rapidly images large specimens via simultaneous light-sheet illumination and fluorescence detection along four orthogonal directions. Combining these four views by means of high-throughput multiview deconvolution yields images with high resolution in all three dimensions. We demonstrate whole-animal functional imaging of *Drosophila* larvae at a spatial resolution of 1.1–2.5 μm and temporal resolution of 2 Hz for several hours. We also present spatially isotropic whole-brain functional imaging in *Danio rerio* larvae and spatially isotropic multicolor imaging of fast cellular dynamics across gastrulating *Drosophila* embryos. Compared with conventional light-sheet microscopy, IsoView microscopy improves spatial resolution at least sevenfold and decreases resolution anisotropy at least threefold. Compared with existing high-resolution light-sheet techniques, IsoView microscopy effectively doubles the penetration depth and provides subsecond temporal resolution for specimens 400-fold larger than could previously be imaged.

Imaging fast processes across large specimens, such as neural activity across the nervous system or cellular dynamics throughout a developing embryo, requires microscopes that provide high speed, high spatial resolution, good physical coverage and low photo-toxicity at the same time. Light-sheet microscopy methods have been developed for high-speed imaging[1,2], but current methods are capable of high-resolution imaging only in small, transparent specimens, such as cultured cells or nematode embryos, or in superficial regions of larger specimens[3,4]. Methods for rapid imaging of larger, less transparent specimens have been proposed as well[5–8] but suffer from low spatial resolution and resolution anisotropy (i.e., the axial resolution is frequently up to tenfold lower than the lateral resolution). These constraints limit the utility of such methods for cellular and subcellular imaging.

Powerful strategies have been proposed for enhancing axial resolution in light-sheet microscopy, focusing on small specimens. One approach utilizes thin light sheets constructed from Bessel beams[9] or optical lattices[3]. However, Bessel-beam light-sheet microscopy increases photo-damage[3,4] by illuminating out-of-focus regions and is thus not well suited to long-term live imaging. Lattice light-sheet microscopy improves resolution using periodic interference patterns, which can be formed with high precision in transparent specimens or at the surfaces of larger samples. In nonsuperficial regions of larger specimens, such as *Drosophila* embryos, the optical lattice is affected by scattering, absorption and aberrations. Consequently, the light sheet broadens in deeper layers, and resolution becomes nonuniform. In *Drosophila* embryos, for example, high-resolution imaging has been demonstrated[3] for depths up to 20 μm. Another important consideration is that reducing the light-sheet thickness affects the maximum temporal resolution: to cover the same volume, more images need to be acquired sequentially. As speed in light-sheet microscopy is limited by camera frame rates[3,5,10–12], this approach decreases temporal resolution and compromises system-level functional imaging, which requires ≥1-Hz sampling[13–15].

Another strategy for resolution enhancement is based on multiview imaging[4,16,17]. The specimen is imaged along multiple directions, which yields multiple relative orientations of the specimen and the microscope's anisotropic point-spread function (PSF). Acquiring two orthogonal views of a sample can be very effective[4]; each individual view is limited by low resolution along a different dimension, but combining both views with multiview deconvolution produces images with high resolution in all dimensions[4,16]. A fast implementation of this strategy, termed dual-view plane illumination (diSPIM)[4], rapidly alternates between light-sheet illumination and fluorescence detection in two orthogonally oriented optical arms. This method is very effective for small, transparent samples and has been demonstrated[4] on volumes up to 80 × 80 × 50 μm^3. However, high-resolution coverage of larger, less transparent samples, such as *Drosophila* embryos or the brains of larval zebrafish, would require imaging of volumes up to 400-fold larger than in previous work, from at least twice as many views[16]. Until now, these requirements could be met only by intrinsically slow, sequential multiview-imaging assays based on physical sample rotation. Although useful for fixed specimens, this method is generally unsuited for rapid live imaging.

Howard Hughes Medical Institute, Janelia Research Campus, Ashburn, Virginia, USA. Correspondence should be addressed to R.K.C. (chhetrir@janelia.hhmi.org) or P.J.K. (kellerp@janelia.hhmi.org).

RECEIVED 8 JULY; ACCEPTED 1 OCTOBER; PUBLISHED ONLINE 26 OCTOBER 2015; DOI:10.1038/NMETH.3632

Here we present IsoView microscopy, which overcomes these limitations by realizing simultaneous four-view imaging and delivers high imaging speed and high spatial resolution for large, live specimens. Using IsoView microscopy, we demonstrated (1) spatially isotropic whole-animal calcium imaging in larval *Drosophila* at 2 Hz, achieving a spatial resolution of 1.1–2.5 µm; (2) spatially isotropic whole-brain functional imaging in larval zebrafish at 1 Hz; and (3) spatially isotropic multicolor imaging of whole gastrulating *Drosophila* embryos at 0.25 Hz. Across all imaging depths, IsoView microscopy improved spatial resolution and resolution isotropy at least sevenfold and threefold, respectively, relative to anisotropic multiview microscopy, without sacrificing imaging speed or long-term imaging capabilities. Compared with previous high-resolution experiments with lattice light-sheet microscopy and diSPIM, IsoView microscopy achieved subsecond temporal resolution for 400-fold larger specimen volumes and effectively doubled the penetration depth. IsoView also enabled—for the first time, to our knowledge—whole-animal functional imaging in larval *Drosophila*, as well as high-resolution, whole-brain functional imaging in

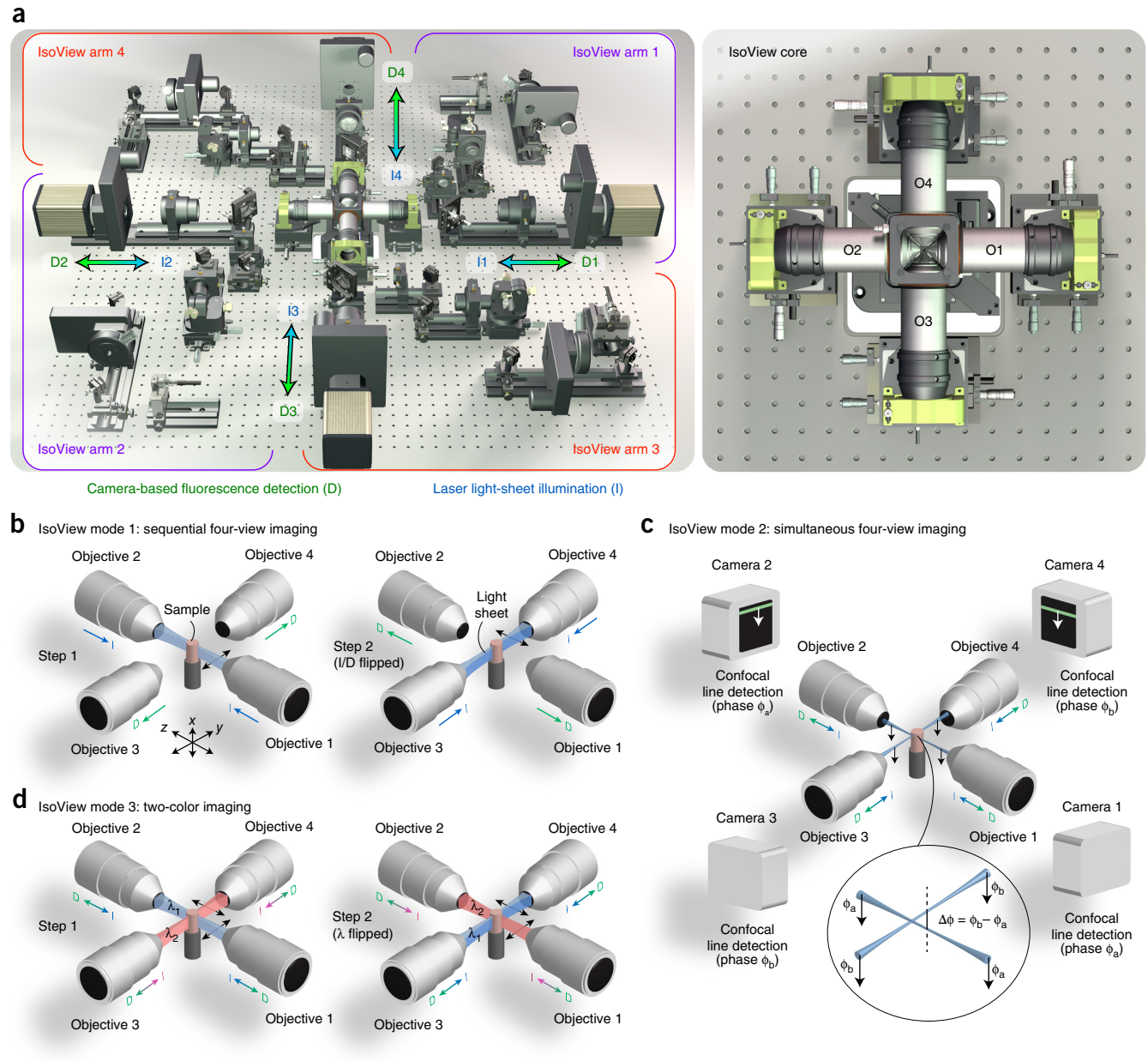

Figure 1 | Isotropic multiview light-sheet microscopy. (**a**) Left, the IsoView microscope consists of four orthogonal arms for simultaneous light-sheet illumination and fluorescence detection. The specimen is located at the center of this arrangement. Volumetric imaging consists of sweeping light sheets across the sample and translating detection planes with objective piezo positioners. Right, top-view close-up of sample chamber, IsoView objectives (O1–O4) and piezo positioners. (**b**–**d**) IsoView imaging modes. In IsoView mode 1 (**b**), four views are acquired by alternating light-sheet illumination (I) and fluorescence detection (D) along orthogonal axes, with temporal separation used to avoid cross-talk between views. In mode 2 (**c**), illumination and detection are performed at the same time in all arms, and cross-talk is avoided via spatially matched beam scanning and confocal detection using a phase offset in orthogonal arms (spatial separation). In mode 3 (**c**), different illumination wavelengths are used in orthogonal arms simultaneously, and four views are acquired for both channels by alternating wavelengths (spectral separation).

larval zebrafish. In these experiments, IsoView microscopy captured neuronal activity at the system level while resolving neighboring cells and other fine morphological features that could not be reliably resolved as distinct structures with state-of-the-art high-speed light-sheet microscopy[5,13].

RESULTS

IsoView light-sheet microscopy

Light-sheet microscopes illuminate a specimen with a sheet of laser light and detect fluorescence emitted by this illuminated section with a wide-field detection system[18–21]. To take advantage of this concept for long-term imaging of large biological specimens with high spatiotemporal resolution, we developed IsoView light-sheet microscopy.

The IsoView microscope consists of four identical, orthogonally arranged optical arms, each of which can simultaneously illuminate the specimen with a scanned laser light sheet[21] and image emitted fluorescence light for a large field of view (**Fig. 1a**, **Supplementary Figs. 1** and **2**, **Supplementary Video 1**, **Supplementary Data 1** and Online Methods). The resulting four orthogonal views of the specimen provide good physical coverage even for relatively large specimens and maximize the volume imaged in high quality from at least two orthogonal views. In such orthogonal views, dimensions along which resolution is high (lateral) and low (axial) are permuted. Fusing the image content from multiple views by means of multiview deconvolution thus yields an image in which resolution is high in all dimensions[4,16].

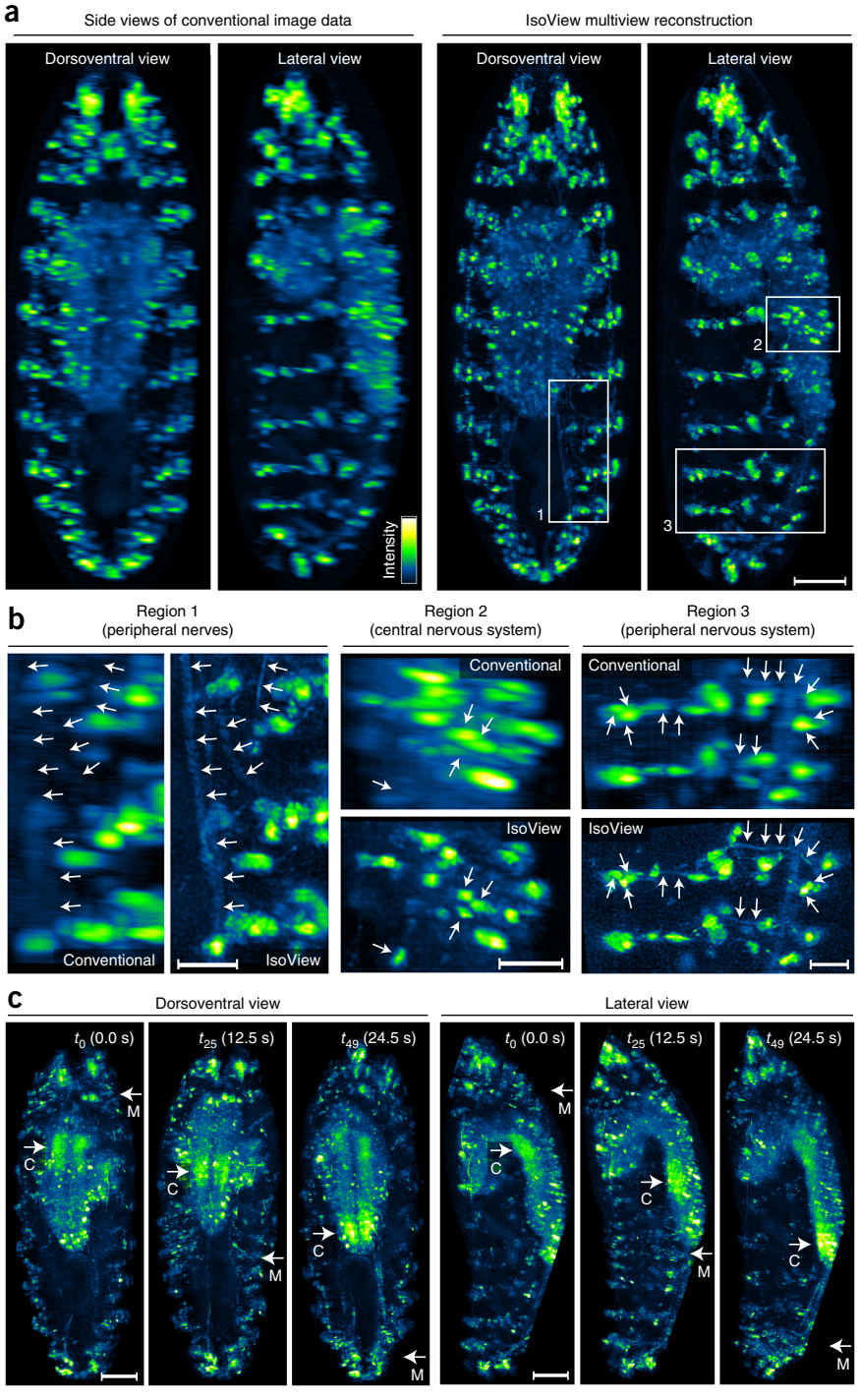

Figure 2 | IsoView whole-animal functional imaging. (**a**) Maximum-intensity projections of conventional and multiview deconvolved IsoView image data of a stage 17 *Drosophila* embryo expressing GCaMP6s throughout the nervous system. The two leftmost panels show side views of image data acquired with two opposing objectives and demonstrate anisotropic resolution in conventional light-sheet microscopy. The two rightmost panels show multiview deconvolution of IsoView four-view data, demonstrating improvements in resolution and isotropy. Rotating views are shown in **Supplementary Video 2**. Four-view data were recorded in 800 ms using IsoView mode 2. A false-color look-up table is used for better visibility of high-dynamic-range images. Signal-to-noise ratio, 211 ± 76 (mean ± s.d., n = 16; Online Methods). Scale bar, 50 µm (scale bar applies to all panels). Boxed regions 1–3 are discussed in subsequent panels. (**b**) Enlarged views of regions highlighted in **a**. Conventional (anisotropic) and IsoView data are shown. Arrows highlight neighboring somas and axons that are not properly resolved in side views of conventional image data. Scale bars, 20 µm (scale bars apply to both images for each region). (**c**) Dorsoventral and lateral projections of multiview deconvolved IsoView data at selected time points t_i of a functional imaging experiment showing calcium dynamics during a backward-locomotion sequence in a *Drosophila* first-instar larva. Arrows labeled "M" indicate waves of muscle contractions traveling anterior to posterior. Arrows labeled "C" indicate waves of calcium activity traveling through the central nervous system concomitant with a wave of muscle contractions. Image data were acquired in IsoView mode 1, providing four-view coverage of the larva at 2 Hz. The complete data set covers a 9-h period in 4.5 million images. Imaging was stopped when the larva crawled out of the imaging volume. **Supplementary Videos 3** and **4** show rotating views and time-lapse visualizations. Scale bars, 50 µm (scale bar applies to all panels for each view).

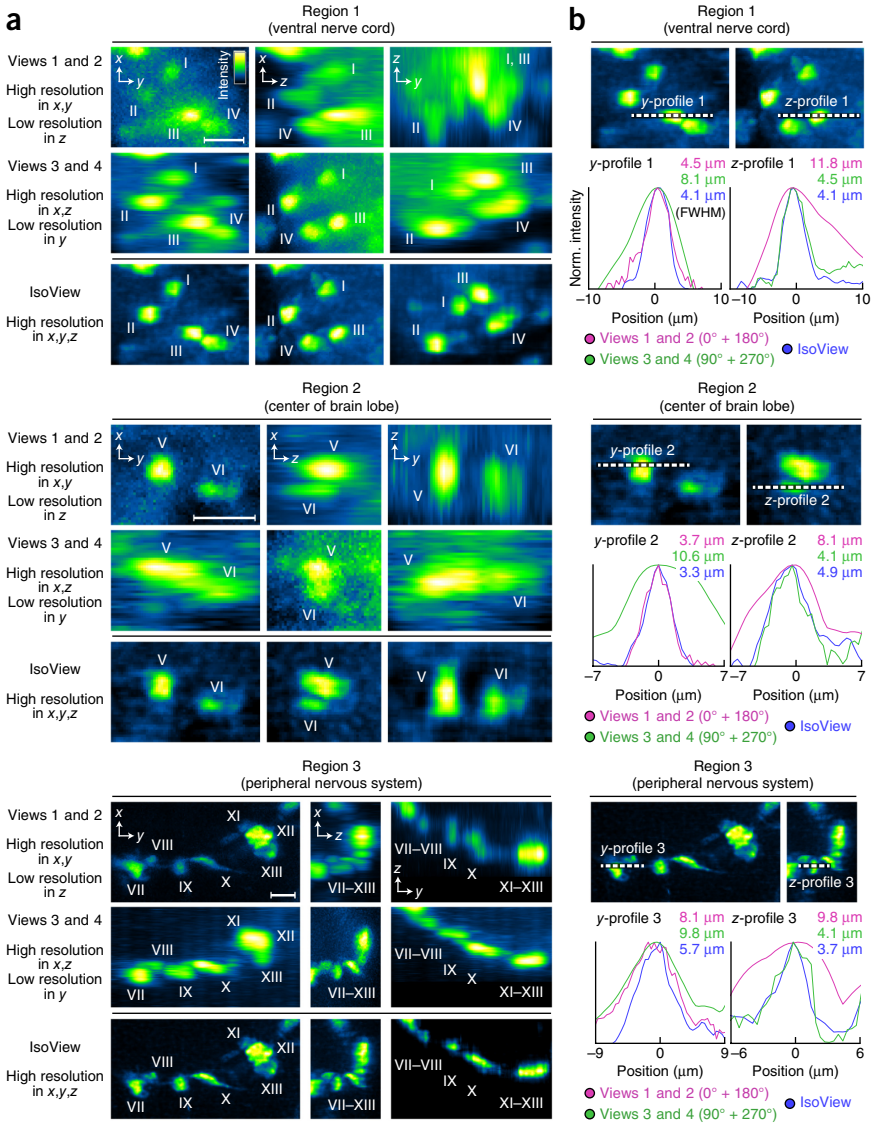

Figure 3 | Improving resolution and isotropy by IsoView functional imaging. (**a**) Side-by-side comparison of raw anisotropic image data and multiview deconvolved IsoView image data for optical sections of the specimen shown in **Figure 2**, using the same false-color look-up table. Examples from different parts of the nervous system are shown. The center of the brain lobe (center) represents one of the deepest and optically most challenging parts of the specimen. Roman numerals identify locations of somas with high GCaMP6s fluorescence. Scale bars, 10 µm (scale bar for each region applies to all images of that region). (**b**) Side-by-side comparison of intensity profiles along *y*- and *z*-axes extracted from the raw anisotropic image data and multiview deconvolved IsoView image data. The location of the line plot in each optical section is indicated by the dashed line in the panels above. Numerical results shown next to the raw intensity profiles represent FWHM size measurements. Note that these FWHM size measurements results do not directly quantify local resolution, as the results have not been corrected for the finite physical size of the analyzed structures (cell somas typically have a diameter of at least 3 µm). *In vivo* resolution estimates based on fluorescently labeled beads are provided in **Supplementary Figure 7**. Norm., normalized.

PSF isotropy is not yet maximized with four views and could in principle be further improved with additional views[16]. However, four-view imaging represents an effective practical solution, as it offers substantial improvements in resolution and isotropy without affecting other critical imaging parameters. Because IsoView microscopy fully parallelizes four-view imaging and operates at the same high volumetric speed as conventional single-view microscopy (as detailed below), this approach provides high temporal resolution and high spatial resolution at the same time.

For imaging of large specimens, IsoView microscopy demands detection optics that offer long working distances, access to a large field of view, and a compact geometrical design suitable for orthogonal four-view imaging. High-speed, long-term imaging also benefits from good lateral resolution and light-collection efficiency and thus demands the highest numerical aperture compatible with these geometrical constraints. Because these specifications are not met by existing commercial optics, we used custom objectives to build the IsoView microscope (**Supplementary Figs. 3–5** and **Supplementary Data 2**), supporting a maximum imaging volume of 800 × 800 × 800 µm^3.

We implemented three IsoView imaging modes that ensured high-quality optical sectioning in all four views without fluorescence contamination from the respective perpendicular views (**Fig. 1b–d**). These modes take advantage of temporal (mode 1), spatial (mode 2) and spectral (mode 3) separation of fluorescence light along orthogonal axes. In mode 1 (**Fig. 1b**), four-view imaging of a single color channel is performed via two fast sequential volumetric scans, using two opposing objectives for sample illumination and the orthogonal objectives for fluorescence detection. Illumination and detection assignments are then alternated in successive scans. Because IsoView optical sectioning is performed with a scanned light sheet[21], the four views can also be acquired simultaneously; in mode 2 (termed phase-shifted confocal line detection; **Fig. 1c**), the four scanned laser beams illuminate the sample simultaneously, using a small scan phase offset in the orthogonal illumination arms. Thus laser beams in orthogonal arms do not cross paths at any time during the plane-illumination process. Fluorescence light is selectively imaged by the four detection systems using confocal line detection[22] with a matched phase delay. Mode 3 is designed for multicolor imaging and enables simultaneous four-view imaging via the use of light sheets at different laser wavelengths along perpendicular optical axes (**Fig. 1d** and **Supplementary Fig. 2**). The principles underlying modes 2 and 3 can be combined, as demonstrated below.

Here we provide a detailed blueprint of the IsoView microscope, including an overview video (**Supplementary Video 1**), technical

drawings (**Supplementary Data 1**), Zemax models of custom optics (**Supplementary Data 2**), a comprehensive parts list (**Supplementary Table 1** and Online Methods), alignment instructions (**Supplementary Note** and **Supplementary Figs. 1–4**) and experimental settings used in this study (**Supplementary Table 2**).

Improving resolution and isotropy in large specimens

To improve resolution and isotropy, the four complementary views captured by the IsoView microscope are registered and combined into a single image volume by multiview deconvolution (**Supplementary Fig. 6a**). Because IsoView microscopy can be applied to a wide spectrum of model systems, marker strategies and imaging assays (as shown below), the strategy underlying image registration should be robust with respect to different types of image content. Performance requirements also include high accuracy, as the magnitude of the improvement in resolution depends on registration accuracy, and high speed, as IsoView is capable of acquisition rates up to 10 terabytes (TB) h^{-1}. To meet these specifications, we developed an automated content-based image-registration method that performs affine registration of all four views simultaneously (Online Methods). For certain types of specimens containing bead-like fluorescent structures, existing registration methods can be used as well[23].

High throughput is equally important during subsequent multiview deconvolution. Although powerful three-dimensional deconvolution methods exist[4,17,24], the fastest method[17] would require several months of computation time on a high-end workstation for a typical multi-TB IsoView data set (Online Methods). We therefore developed a custom implementation of the Lucy-Richardson multiview deconvolution algorithm that speeds up processing by >20-fold using a single graphics processing unit (GPU) and by >60-fold using a multi-GPU workstation (Online Methods). Our software is entirely CUDA-based, which allows us to take full advantage of CUDA fast Fourier transform libraries and fast pixelwise operations while minimizing communication overhead between central processing unit (CPU) and GPU (Online Methods). Thus three-dimensional deconvolution can be performed in approximately 2 d for data volumes on the order of 10 TB (**Supplementary Fig. 6b**), without any loss of accuracy or image quality.

To characterize the resulting spatial resolution in IsoView microscopy, we performed two experiments. First we measured single-view and multiview deconvolved system PSFs with fluorescent beads under mildly light-scattering conditions. Full-width at half-maximum (FWHM) sizes decreased from 0.60 ± 0.03 µm (laterally) and 2.98 ± 0.29 µm (axially) in single-view PSFs to 0.42 ± 0.02 µm (laterally and axially) in multiview deconvolved PSFs (mean ± s.d., $n = 26$; **Supplementary Fig. 6c**). Resolution (PSF volume) and anisotropy in the multiview deconvolved images were thus improved 14- and 18-fold, respectively (Online Methods). Second, we measured PSFs *in vivo* by imaging fluorescent beads injected at different depths in live stage 17 *Drosophila* embryos (**Supplementary Fig. 7**). In superficial tissues, IsoView microscopy improved PSF sizes from 1.77 to 1.09 µm lateral-vertically, from 2.06 to 1.68 µm lateral-horizontally and from 5.45 to 1.59 µm axially ($n = 4$, s.d. < 19% in all cases). Near the center of the embryo, IsoView microscopy

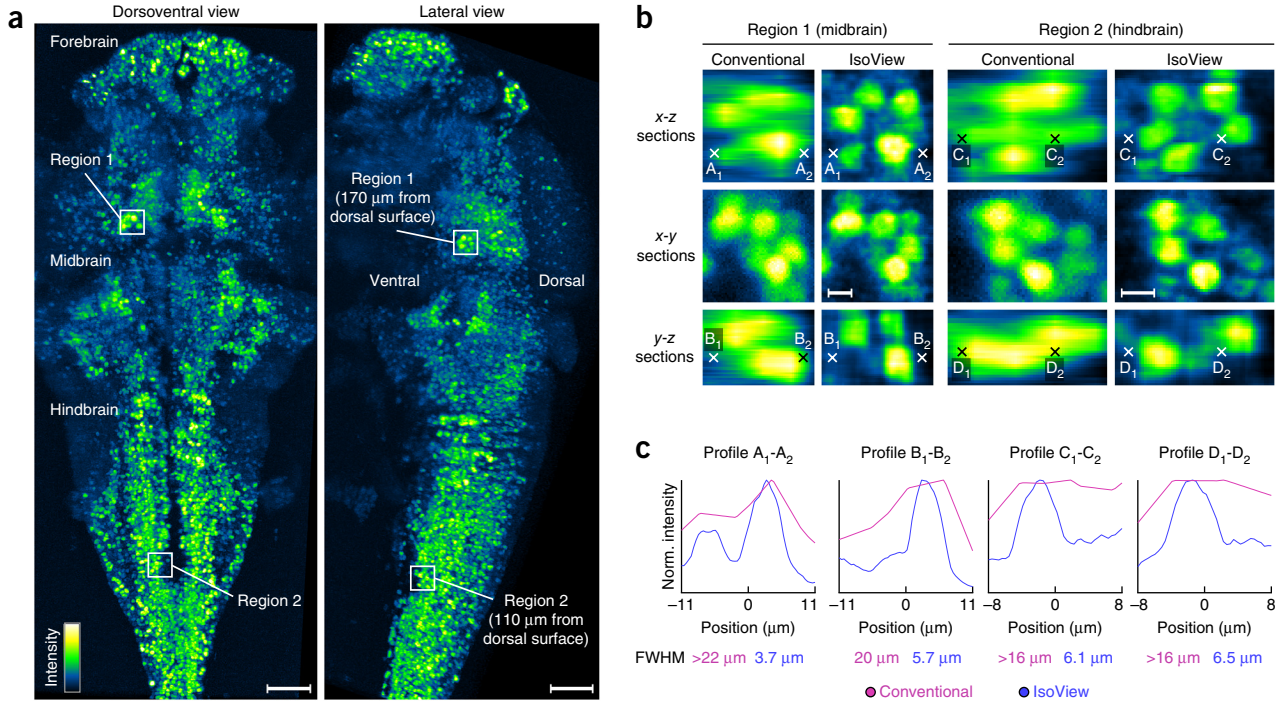

Figure 4 | IsoView whole-brain functional imaging in larval zebrafish. (**a**) Dorsoventral and lateral projections of IsoView functional imaging data of the brain of a 3-d-old larval zebrafish expressing nuclear-localized GCaMP6 throughout its nervous system. **Supplementary Video 5** shows a time-lapse visualization. Scale bars, 50 µm. (**b**) Side-by-side comparison of conventional image data (acquired according to the functional imaging approach introduced by Ahrens *et al.*[13]) and multiview deconvolved IsoView image data for *x-y*, *x-z* and *y-z* slices from the two deep-tissue image regions highlighted in **a**. Optical path lengths inside the brain relative to lateral and dorsal surfaces were 140 µm and 170 µm for region 1 and 80 µm and 110 µm for region 2. Scale bars, 5 µm (scale bar for each region applies to all images of that region). (**c**) Side-by-side comparison of intensity profiles in conventional image data and multiview deconvolved IsoView image data for the four linear segments (A_1-A_2, B_1-B_2, C_1-C_2 and D_1-D_2) indicated in **b**. Note that FWHM size measurements results do not directly quantify local resolution, as the results have not been corrected for the finite physical size of the analyzed structures (cell somas typically have a diameter of at least 3 µm).

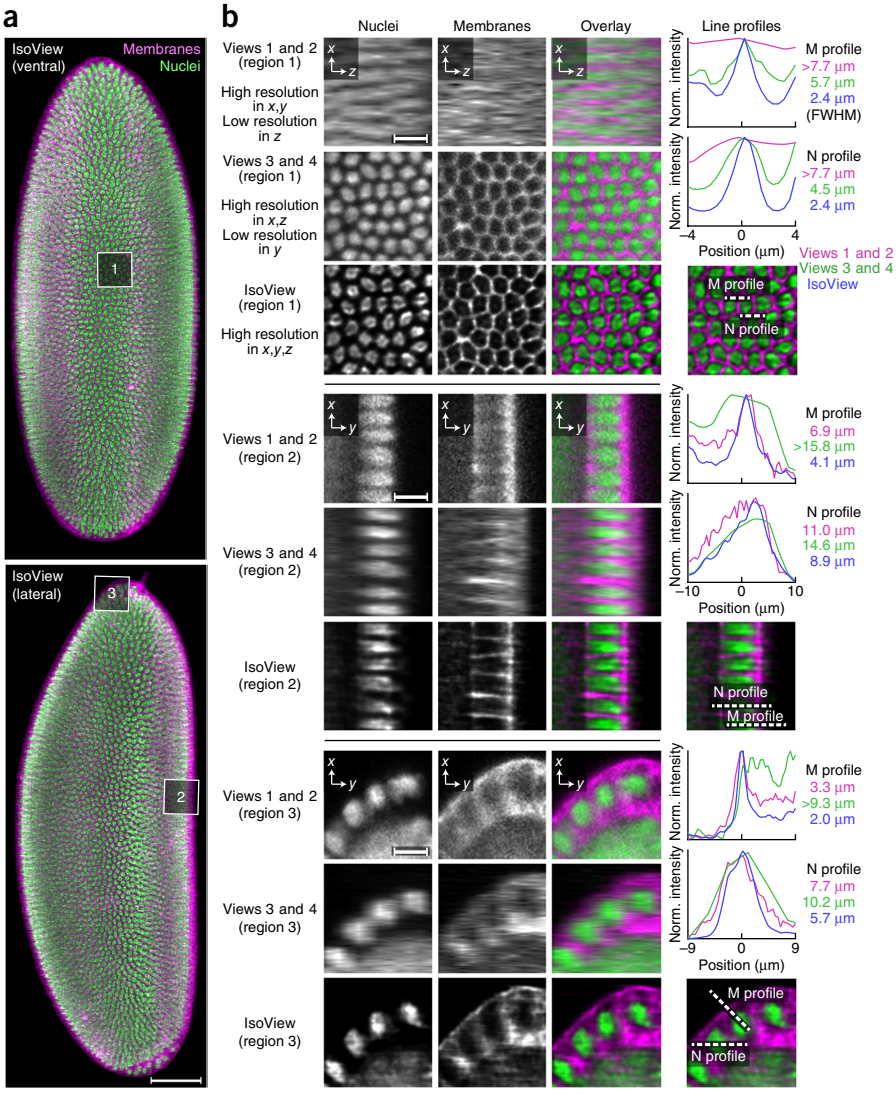

Figure 5 | Improving resolution and isotropy by IsoView developmental imaging. (**a**) Ventral- and lateral-view maximum-intensity projections of multiview deconvolved IsoView image data of a stage 5 *Drosophila* embryo during cellularization of the blastoderm. Four-view, two-color imaging of fluorescently labeled nuclei (His2Av-mRFP1) and membranes (Spider-GFP) was performed with a combination of IsoView modes 2 and 3 (four-view, two-color imaging with phase-shifted confocal detection in orthogonal arms). Colors are inverted for better visibility. The snapshots represent a single time point from an IsoView time-lapse recording of *Drosophila* gastrulation at 0.25-Hz temporal resolution (**Supplementary Video 7**). The signal-to-noise ratio was 132 ± 43, mean ± s.d., $n = 8$ (Online Methods). **Supplementary Video 6** shows a detailed three-dimensional visualization of the image data. Boxed regions 1–3 are discussed in subsequent panels. Scale bar, 50 µm (applies to both images). (**b**) Side-by-side comparison of raw anisotropic image data and IsoView image data for various optical sections of the embryo shown in **a**. Shown are examples from different parts of the embryo: ventral (region 1), dorsal (region 2) and anterior (region 3) parts of the blastoderm. Graphs at right show side-by-side comparisons of intensity profiles from nuclei (N profiles) and membrane (M profiles) channels along *y*- and *z*-axes of the image data. The locations of the line plots in each optical section are indicated by dashed lines in the image panels below the plots. Numerical results shown next to the raw intensity profiles represent FWHM size measurements. Scale bars, 10 µm (scale bar for each region applies to all images of that region).

improved PSF sizes from 2.24 to 1.20 µm lateral-vertically, from 2.60 to 1.73 µm lateral-horizontally and from 7.41 to 2.13 µm axially ($n = 4$, s.d. < 40% in all cases). PSF volumes *in vivo* were thus improved sevenfold to tenfold and resolution anisotropy was reduced threefold to fourfold in the multiview deconvolved images compared with the single-view images. Although spatial resolution gradually decreased with increasing imaging depth, IsoView PSFs exhibited good isotropy independent of depth. For most of the embryo, resolution was in the range of 1.1–1.7 µm. The deepest and optically least accessible parts could still be imaged at a resolution of 2.5 µm or better (**Supplementary Fig. 7**).

Finally, we compared high-resolution coverage in a live *Drosophila* embryo for orthogonal dual- and four-view imaging (**Supplementary Figs. 8–10**). Orthogonal dual-view imaging provided excellent resolution up to a depth of ~60 µm, covering approximately one-quarter of the specimen; for illumination and detection paths exceeding 60 µm in length, resolution and signal strength degraded substantially, and cellular resolution was typically compromised. In contrast, high-resolution coverage of almost the entire embryo was achieved with four-view imaging, which is consistent with the expectation that the acquisition of opposing views in IsoView microscopy should effectively double the penetration depth. Notably, four-view imaging still resolved neighboring cell nuclei as distinct objects in some of the deepest regions of the embryo with path lengths approaching 100 µm.

To demonstrate the capabilities of IsoView microscopy in high-resolution imaging of fast biological processes, we performed whole-animal functional imaging in embryonic and larval *Drosophila* (**Figs. 2** and **3** and **Supplementary Videos 2–4**), whole-brain functional imaging in larval zebrafish (**Fig. 4** and **Supplementary Video 5**) and whole-animal multicolor imaging of developing *Drosophila* embryos (**Figs. 5** and **6** and **Supplementary Videos 6** and **7**).

High-resolution whole-animal functional imaging

The generation of coordinated behaviors relies on communication between large populations of neurons in widely separated parts of the central and peripheral nervous systems. Our understanding of these complex, dynamic processes would benefit substantially from knowledge of neural activity throughout the nervous system. To demonstrate how IsoView can provide such system-level data at high spatiotemporal resolution, we performed whole-animal functional imaging of stage 17 *Drosophila* embryos expressing the calcium indicator GCaMP6s (**Fig. 2** and Online Methods). Using

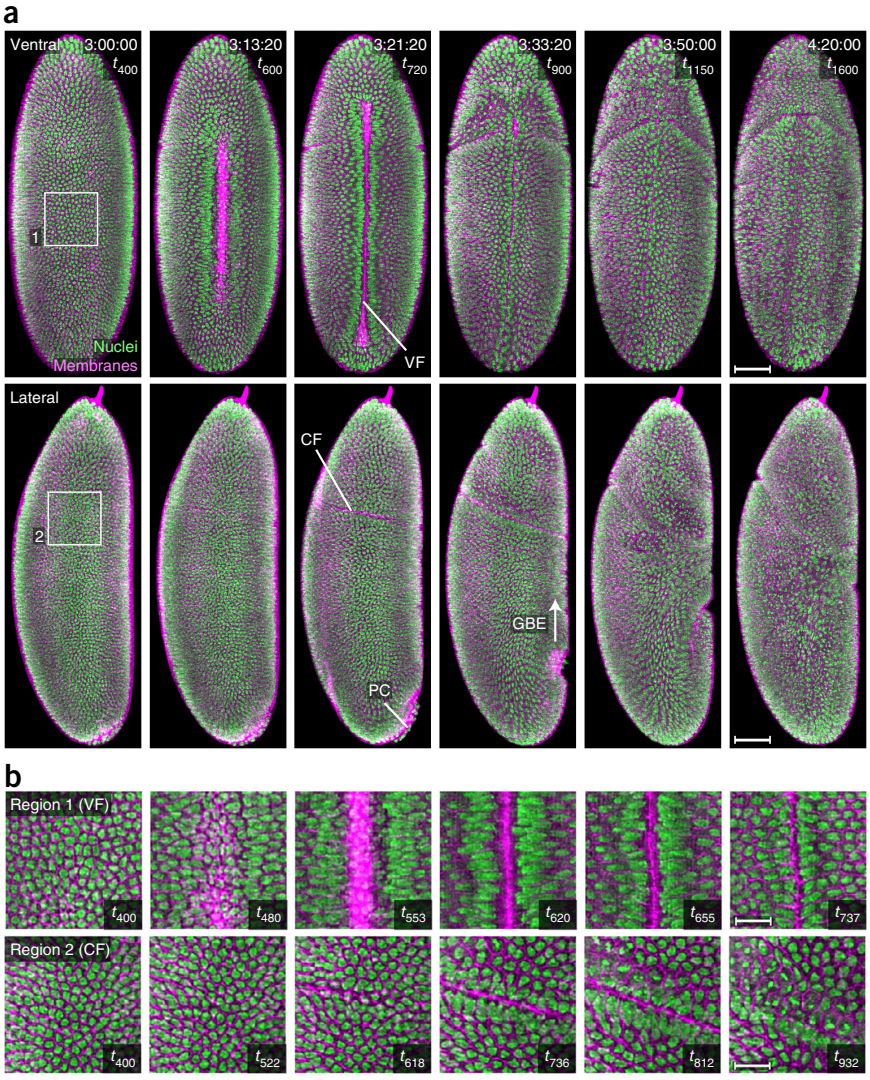

Figure 6 | Multicolor imaging of whole-embryo development with isotropic spatial resolution. (**a**) Ventral (top row) and lateral (bottom row) views of multiview deconvolved IsoView image data of a gastrulating *Drosophila* embryo at selected time points t_i. Four-view two-color imaging of fluorescently labeled nuclei (His2Av-mRFP1) and membranes (Spider-GFP) was performed with a combination of IsoView modes 2 and 3 (four-view, two-color imaging with phase-shifted confocal detection in orthogonal arms). Colors are inverted for better visibility. **Supplementary Video 7** shows time-lapse visualizations, including static and rotating views. Scale bars, 50 µm (scale bars apply to all images in their respective rows). (**b**) Enlarged views of the two regions highlighted in **a**, showing ventral furrow formation (region 1, ventral view) and cephalic furrow formation (region 2, lateral view). VF, ventral furrow; CF, cephalic furrow; PC, pole cells; GBE, germ-band extension. Scale bars, 20 µm (scale bars apply to all images in their respective rows).

IsoView modes 1 and 2 (**Fig. 1b**,**c**), we achieved sustained four-view volumetric imaging speeds of 2 and 1 Hz, respectively, and captured whole-nervous-system activity patterns underlying various locomotor behaviors such as forward crawling, backward crawling and turning (**Fig. 2** and **Supplementary Video 3**). Signal fidelity and noise statistics in IsoView functional traces of individual neurons were similar to the average values for the respective two best single views (**Supplementary Fig. 11**). Spatial resolution was improved substantially throughout the nervous system, revealing axons, axon bundles and neighboring cell somas that could not be resolved as distinct structures with conventional light-sheet imaging (**Figs. 2b** and **3**, **Supplementary Fig. 12** and **Supplementary Video 2**). We also investigated improvements in resolution and isotropy during fast specimen movements, selecting forward locomotion as a challenging test case, and found that IsoView image registration achieved high accuracy for imaging speeds of 2 Hz (**Supplementary Fig. 13**). Finally, we assessed IsoView's long-term functional imaging capabilities by recording a stage 17 *Drosophila* embryo as it developed into a first-instar larva (**Supplementary Video 4**). We performed 2-Hz functional imaging over a period of 9 h with 50% duty cycle. At the end of the experiment, the fully formed larva crawled out of the imaging volume (**Supplementary Video 4**). More than 120,000 single-view image volumes (4.5 million images) were acquired for this specimen, with minimal photo-bleaching (**Supplementary Video 4**), resulting in more than 30,000 multiview deconvolved high-resolution IsoView image stacks.

High-resolution zebrafish whole-brain functional imaging

IsoView microscopy also facilitates high-resolution functional imaging of even larger specimens. To demonstrate this, we acquired IsoView calcium-imaging data of the entire head region of a 3-d-old larval zebrafish expressing nuclear-localized GCaMP6s (Online Methods)[10]. Using IsoView mode 1, we acquired four-view whole-brain imaging data of the 800 × 400 × 400 µm^3 volume at 1 Hz (**Fig. 4a** and **Supplementary Video 5**), capturing large-scale brain activity related to motor behaviors of the awake animal (**Supplementary Video 5**). Improvements in resolution, isotropy and physical coverage were similar to those observed in IsoView experiments with *Drosophila* (**Fig. 4b**,**c**). Unlike conventional light-sheet functional imaging[13], IsoView microscopy was able to reliably resolve neighboring cell nuclei as distinct objects in some of the deepest regions of mid- and hindbrain (**Fig. 4**).

High-resolution two-color imaging of fruit fly development

As a third demonstration, we used a combination of IsoView modes 2 and 3 for two-color imaging of developing *Drosophila* embryos undergoing gastrulation (Online Methods). This approach captured two-color four-view image data at a volumetric rate of 0.25 Hz and reliably discerned neighboring cells and subcellular morphological features throughout the blastoderm (**Fig. 5**, **Supplementary Figs. 14** and **15** and **Supplementary Video 6**). In contrast, conventional light-sheet microscopy lacked subcellular resolution in many regions of the embryo and frequently failed to resolve neighboring cells as distinct objects (**Fig. 5b** and **Supplementary Video 6**). IsoView microscopy provided near-isotropic spatial

resolution, long-term imaging capability (covering a 3-h developmental period with 1.6 million images; **Fig. 6**) and good temporal sampling of fast cellular dynamics, such as changes in cell morphology across the embryo during ventral furrow invagination and the rapid dorsally directed movement of the posterior pole cells during germ-band extension (**Supplementary Video 7**).

DISCUSSION

A key strength of IsoView microscopy is that it provides good temporal resolution, spatial resolution, isotropy, physical coverage and long-term imaging capability at the same time, even for relatively large live specimens. Most important, IsoView improves the spatial resolution and physical coverage of large specimens without a corresponding loss of temporal resolution. These capabilities are essential for high-resolution imaging of cellular dynamics across developing embryos and for functional imaging of large populations of neurons. Unlike conventional large-scale functional imaging assays[2,5,13–15], which provide high imaging speed but suffer from low resolution and isotropy, IsoView microscopy reliably distinguishes neighboring cells and resolves neuronal morphologies[5] even in deep-tissue regions. Moreover, IsoView enabled functional imaging of an entire behaving animal with a fairly complex nervous system comprising more than 10,000 neurons.

To support the dissemination of IsoView microscopy, we have provided the IsoView blueprint, detailed technical information and the open source code of our IsoView multiview deconvolution software. We anticipate that the powerful combination of high temporal resolution and high spatial resolution offered by IsoView microscopy will open the door to a wide range of live-imaging applications throughout the life sciences, from high-resolution imaging of fast developmental processes at the whole-organism level, such as changes in cell shape and collective cell movements underlying early embryogenesis, to high-resolution functional imaging of large neuronal populations and even entire nervous system of higher invertebrates and small vertebrates.

METHODS

Methods and any associated references are available in the online version of the paper.

Note: Any Supplementary Information and Source Data files are available in the online version of the paper.

ACKNOWLEDGMENTS

We thank B. Coop and the Janelia ID&F Team for mechanical designs and custom mechanical parts; M. Coleman for custom microscope-operating software; V. Stamataki for help with bead injections in live *Drosophila* embryos and larvae; E. Betzig, K. Branson and G. Rubin for helpful discussions; M. Ahrens and C.-T. Yang (Janelia Research Campus, Ashburn, Virginia, USA) for the GCaMP6s zebrafish line; E. Wieschaus (Howard Hughes Medical Institute, Princeton University, Princeton, New Jersey, USA) for the Spider-GFP flies; the Janelia Fly Facility (Janelia Research Campus, Ashburn, Virginia, USA) for sharing and maintaining transgenic *Drosophila* stocks; and the Janelia Vivarium Team for zebrafish animal care. This work was supported by the Howard Hughes Medical Institute.

AUTHOR CONTRIBUTIONS

P.J.K. and R.K.C. designed the IsoView microscope. R.K.C. built the IsoView microscope and performed all imaging experiments. F.A. developed the IsoView image-processing framework. Y.W. and W.C.L. prepared *Drosophila* specimens for IsoView imaging. B.H. prepared zebrafish specimens for IsoView imaging. P.J.K. conceived of the research, supervised the project and wrote the paper, with contributions from R.K.C.

COMPETING FINANCIAL INTERESTS

The authors declare competing financial interests: details are available in the online version of the paper.

1. Winter, P.W. & Shroff, H. Faster fluorescence microscopy: advances in high speed biological imaging. *Curr. Opin. Chem. Biol.* **20**, 46–53 (2014).
2. Keller, P.J. & Ahrens, M.B. Visualizing whole-brain activity and development at the single-cell level using light-sheet microscopy. *Neuron* **85**, 462–483 (2015).
3. Chen, B.C. *et al.* Lattice light-sheet microscopy: imaging molecules to embryos at high spatiotemporal resolution. *Science* **346**, 1257998 (2014).
4. Wu, Y. *et al.* Spatially isotropic four-dimensional imaging with dual-view plane illumination microscopy. *Nat. Biotechnol.* **31**, 1032–1038 (2013).
5. Lemon, W.C. *et al.* Whole-central nervous system functional imaging in larval *Drosophila*. *Nat. Commun.* **6**, 7924 (2015).
6. Tomer, R., Khairy, K., Amat, F. & Keller, P.J. Quantitative high-speed imaging of entire developing embryos with simultaneous multiview light-sheet microscopy. *Nat. Methods* **9**, 755–763 (2012).
7. Krzic, U., Gunther, S., Saunders, T.E., Streichan, S.J. & Hufnagel, L. Multiview light-sheet microscope for rapid *in toto* imaging. *Nat. Methods* **9**, 730–733 (2012).
8. Schmid, B. *et al.* High-speed panoramic light-sheet microscopy reveals global endodermal cell dynamics. *Nat. Commun.* **4**, 2207 (2013).
9. Planchon, T.A. *et al.* Rapid three-dimensional isotropic imaging of living cells using Bessel beam plane illumination. *Nat. Methods* **8**, 417–423 (2011).
10. Vladimirov, N. *et al.* Light-sheet functional imaging in fictively behaving zebrafish. *Nat. Methods* **11**, 883–884 (2014).
11. Mickoleit, M. *et al.* High-resolution reconstruction of the beating zebrafish heart. *Nat. Methods* **11**, 919–922 (2014).
12. Bouchard, M.B. *et al.* Swept confocally-aligned planar excitation (SCAPE) microscopy for high speed volumetric imaging of behaving organisms. *Nat. Photonics* **9**, 113–119 (2015).
13. Ahrens, M.B., Orger, M.B., Robson, D.N., Li, J.M. & Keller, P.J. Whole-brain functional imaging at cellular resolution using light-sheet microscopy. *Nat. Methods* **10**, 413–420 (2013).
14. Panier, T. *et al.* Fast functional imaging of multiple brain regions in intact zebrafish larvae using selective plane illumination microscopy. *Front. Neural Circuits* **7**, 65 (2013).
15. Wolf, S. *et al.* Whole-brain functional imaging with two-photon light-sheet microscopy. *Nat. Methods* **12**, 379–380 (2015).
16. Swoger, J., Verveer, P., Greger, K., Huisken, J. & Stelzer, E.H. Multi-view image fusion improves resolution in three-dimensional microscopy. *Opt. Express* **15**, 8029–8042 (2007).
17. Preibisch, S. *et al.* Efficient Bayesian-based multiview deconvolution. *Nat. Methods* **11**, 645–648 (2014).
18. Voie, A.H., Burns, D.H. & Spelman, F.A. Orthogonal-plane fluorescence optical sectioning: three-dimensional imaging of macroscopic biological specimens. *J. Microsc.* **170**, 229–236 (1993).
19. Fuchs, E., Jaffe, J., Long, R. & Azam, F. Thin laser light sheet microscope for microbial oceanography. *Opt. Express* **10**, 145–154 (2002).
20. Huisken, J., Swoger, J., Del Bene, F., Wittbrodt, J. & Stelzer, E.H.K. Optical sectioning deep inside live embryos by selective plane illumination microscopy. *Science* **305**, 1007–1009 (2004).
21. Keller, P.J., Schmidt, A.D., Wittbrodt, J. & Stelzer, E.H.K. Reconstruction of zebrafish early embryonic development by scanned light sheet microscopy. *Science* **322**, 1065–1069 (2008).
22. Baumgart, E. & Kubitscheck, U. Scanned light sheet microscopy with confocal slit detection. *Opt. Express* **20**, 21805–21814 (2012).
23. Preibisch, S., Saalfeld, S., Schindelin, J. & Tomancak, P. Software for bead-based registration of selective plane illumination microscopy data. *Nat. Methods* **7**, 418–419 (2010).
24. Temerinac-Ott, M., Ronneberger, O., Nitschke, R., Driever, W. & Burkhardt, H. Spatially-variant Lucy-Richardson deconvolution for multiview fusion of microscopic 3D images. In *Proc. IEEE International Symposium on Biomedical Imaging* 899–904 (IEEE, 2011).

ONLINE METHODS

IsoView light-sheet microscope. The IsoView microscope consists of two custom SOLE-6 multilaser units, four scanned light-sheet illumination arms, four fluorescence-detection arms equipped with sCMOS (scientific complementary metal-oxide semiconductor) cameras, a custom four-view specimen chamber and a four-axis specimen-positioning system that is magnetically connected to the specimen holder in the specimen chamber (**Supplementary Table 1**). Each SOLE-6 unit (Omicron Laserage) has two exit ports at which the multilaser beams (488 nm, 515 nm, 561 nm and 594 nm) are guided through two single-mode fibers onto two illumination arms for fluorescence excitation. Each illumination arm consists of a fiber-to-free-space collimator, a compact illumination-filter wheel (96A351, Ludl) with controller (MAC6000 DC servo controller, Ludl), a high-speed laser shutter with controller (VS14S2ZM1-100 with AlMgF2 coating, VMM-D3 three-channel driver, Uniblitz), a pair of de-magnifying relay lenses (49-363-INK and 49-356-INK, Edmund Optics), a dual-axis galvanometer scanner (6215HSM40B with 673XX dual-axis driver, Cambridge Technology), a custom f-θ lens (55-S96-16T, Special Optics), an illumination tube lens (49-363-INK, Edmund Optics), a dichroic beam splitter (zt488/561rpc or zt488/594rpc, Chroma), and a custom water-dipping objective (54-23-15, Special Optics) mounted atop a linear-translation piezo (P-622.1CD or P-628.1CD PIHera stage with E-709.CHG digital controller, Physik Instrumente). The illumination-filter wheel contains various illumination filters (neutral-density filters, Chroma; laser cleanup notch filters, Melles Griot). Each detection arm shares the water-dipping custom objective and the dichroic beam splitter and additionally consists of a detection-filter wheel with an internal shutter (96A354, Ludl) with its controller shared with the illumination-filter wheel in the same arm, a custom tube lens (55-S240-16T, Special Optics), and an sCMOS camera (Orca Flash 4.0 v2, Hamamatsu). The detection-filter wheel contains various detection filters (BrightLine long-pass and band-pass filters, Semrock). The four-view specimen chamber comprises a custom specimen holder made of medical-grade stainless steel, a custom mechanical scaffold manufactured from black Delrin, a multistage adaptor module to connect the specimen holder and a four-axis specimen positioning system, four custom water seals made of silicone to seal the spacing between the objectives and the chamber, and another water seal to close the gap on the underside of the chamber through which the specimen holder is inserted. With the four-axis specimen-positioning system, the specimen holder can be translated in three dimensions and rotated around its main axis without breaking the water seal. The top of the chamber is open for mechanical access and also allows for background illumination with a cold light source during sample positioning. The four-axis (x-y-z-θ) specimen-positioning system consists of three customized translation stages (M-111K046, Physik Instrumente) and one rotary stage (M-116.2DG, Physik Instrumente) controlled by a motion controller (C-884.4D, Physik Instrumente).

A schematic outline of the IsoView microscope is shown in **Supplementary Figure 1**, and technical drawings of the IsoView custom optical components are shown in **Supplementary Figure 3**. A comprehensive list of IsoView components is provided in **Supplementary Table 1**. Additionally, a detailed alignment procedure for the IsoView microscope is provided in the **Supplementary Note**, and technical drawings of the IsoView custom mechanical components and Zemax models of the IsoView custom optics are provided as **Supplementary Data 1** and **2**, respectively.

IsoView electronics and control framework. The optical and mechanical components of the IsoView microscope are operated and synchronized by four field programmable gated arrays (FPGAs) housed in a PXI bus extender chassis (PXI-1065, National Instruments). Collectively, the four FPGAs provide 32 analog output, 32 analog input and 382 digital input-output channels. The FPGAs are interfaced via high-performance shielded cables (SHC68-68-RMIO, National Instruments) to 68-terminal connector blocks (CB-68LPR, National Instruments) housed in configurable enclosures (CA-1000, National Instruments), which are extended via BNC (Bayonet Neill–Concelman) panelettes for connections to the IsoView control devices. The filter wheels in the IsoView microscope are controlled by a four-port serial-interface board (PXI-8430/4, National Instruments) in the PXI-1065 chassis. Direct control of the FPGAs and the serial-interface board by the microscope-control workstation is enabled by the controller for PXI/PXIe modules (PXIe/PCIe-8381, National Instruments), housed in the PXI-1065 chassis.

The PXI bus extended chassis is connected to the IsoView control computer, which operates the four sCMOS cameras and runs the custom IsoView control software, written in LabVIEW (National Instruments). The IsoView control computer is equipped with two Xeon E5-2687WV2 CPUs (Intel), 256 GB of DDR-3 memory, four FireBird CameraLink frame grabbers (Active Silicon), two Adaptec 24-channel 72405 RAID controllers, 22 Samsung 840 EVO 1-TB solid-state drives combined into two 11-TB RAID-0 data arrays for simultaneous high-speed image-data streaming from four sCMOS cameras at a total data rate of up to 3.2 GB/s, and an X520-SR1 SFP+ SR LC fiber network adaptor (Intel) for transferring IsoView image data to the IsoView image server. The IsoView image server is based on a SuperMicro SuperStorage 5048R-E1CR36L server platform and is equipped with a Xeon E5-2630V3 CPU (Intel), 128 GB of DDR-3 memory, an LSI 9361-9i eight-channel RAID controller, 36 Seagate Constellation ES.4 6-TB hard disks combined into two RAID-6 data arrays with a total storage capacity of 175 TB, and an X520-SR1 SFP+ SR LC fiber network adaptor (Intel) for data transfer between the IsoView control computer and image server. The IsoView control computer and image server run Windows 7 Professional 64-bit and Windows 2012 Server (Microsoft), respectively.

IsoView sample preparation. *Drosophila* functional-imaging experiments were performed with embryos and first-instar larvae expressing the calcium indicator[25] UAS-GCaMP6s under control of the elav-Gal4 driver (elav-Gal4/+; 10× UAS-GCaMP6s/+; +). Developmental-imaging experiments were performed with embryos that had homozygous labels in nuclei and membranes (w; His2Av-mRFP1; Spider-GFP)[26,27]. The parental flies were placed in a mating cage for 2 h, where they deposited embryos on the surface of a culture dish filled with agar prepared with a solution of 50% grape juice. The embryos were dechorionated with a 30-s exposure to 50% sodium hypochlorite solution (Sigma-Aldrich, 425044), rinsed in tap water and washed into a plastic culture dish. The fluorescent embryos were briefly screened with a fluorescence dissecting microscope so that individual embryos of the appropriate age could be selected for imaging (<2 h after egg

laying for developmental imaging, and 18–20 h after egg laying for calcium imaging). The selected embryos were then embedded in 1.2% low-melting-temperature agarose (Lonza, SeaPlaque) at 36 °C in a 1.5 mm inner diameter × 20 mm glass capillary (Hilgenberg) with the anterior-posterior axis of the embryo parallel to the long axis of the capillary. Each embryo was positioned in the center of the capillary bore and repositioned frequently with the tip of #5 forceps while the agarose cooled. After a few minutes, the fully gelled cylinder of agarose was pushed out of the capillary just enough to expose the embryo outside of the glass. The capillary holding the embryo was positioned vertically in the sample holder at the center of the water-filled recording chamber of the IsoView microscope so that the specimen was supported from below by agarose and all four objectives had unobstructed optical access to the specimen.

Zebrafish experiments were conducted according to protocols approved by the Institutional Animal Care and Use Committee of the Howard Hughes Medical Institute, Janelia Research Campus. At 2.5 d post-fertilization (dpf), zebrafish larvae expressing nuclear-localized GCaMP6s driven by the HuC promoter[10] were paralyzed by brief exposure to 1 mg ml^{-1} α-bungarotoxin solution (Life Technologies) and embedded in 1.0% low-melting-temperature agarose (Lonza, SeaPlaque) inside 1.5 mm inner diameter × 20 mm glass capillaries (Hilgenberg). During gelling of the agarose, the fish was aligned and centered inside the glass capillary by rotation of the capillary and gentle manipulation with Microloader tips (Eppendorf). Just before insertion of the capillary into the microscope sample holder, the fish was positioned above the rim of the glass capillary by extrusion of the agarose cylinder.

The figures, videos and analyses presented in this study are based on image data from $n = 8$ specimens, including four functional-imaging experiments in late embryonic and early larval *Drosophila* (embryonic stage 17 to larval stage L1), one functional-imaging experiment in larval zebrafish (3 dpf), one developmental-imaging experiment in early embryonic *Drosophila* (embryonic stages 6–8), one recording of a *Drosophila* embryo ubiquitously expressing nuclear markers (embryonic stage 17) using orthogonal dual-view and four-view imaging, and one recording of fluorescent beads injected in a live *Drosophila* embryo (embryonic stage 17). The sexes of the imaged animals are unknown.

IsoView live imaging. Conceptually, IsoView volumetric imaging is achieved by (1) simultaneous lateral movement of opposing scanned light sheets to illuminate thin slices of the sample and (2) synchronous motion of the orthogonal detection objectives mounted atop piezo linear stages to maintain co-planarity of detection focal planes with these light sheets. The custom water-dipping objectives perform both illumination of the sample and detection of the fluorescence light excited by orthogonal light sheets, with a dichroic beam splitter separating the illumination and detection paths in each of the four arms (**Supplementary Fig. 1**).

The IsoView four-objective configuration with simultaneous illumination and detection capabilities and the use of scanned light sheets[21] enable a range of imaging modes (**Fig. 1b–d**), all of which ensure high-quality optical sectioning without fluorescent light contamination from the respective perpendicular views. Below we describe the three primary imaging modes, which are based on temporal, spatial and spectral separation principles, respectively, for acquisition of four uncontaminated, orthogonal views. Each mode offers distinct advantages and capabilities.

Mode 1: sequential four-view imaging. In this mode, four-view imaging of a single color channel is performed via two fast sequential volumetric scans, using two opposing objectives for sample illumination and two objectives in the orthogonal arms for fluorescence detection. Illumination and detection tasks are then alternated in successive scans. This mode thus temporally separates fluorescence detection in orthogonal arms. This mode uses the sCMOS cameras in rolling-center mode, in which camera exposure starts row by row in a wave moving from the center row of the camera chip to the edges of the chip. Once a sufficiently large area of the chip has been activated in this manner (effectively acting as a global shutter), a rapidly scanned light sheet in the region corresponding to the exposed camera pixels triggers the emission of fluorescence light, which in turn is detected by the cameras. This mode offers particularly high IsoView imaging speeds, as the sCMOS cameras can be oriented so that the exposure wave-propagation direction is aligned with the shorter lateral dimension of the sample, thereby minimizing the time needed to image the region of interest. In this mode, speed is dictated by sample size along the sample's shorter, lateral dimension. For the *Drosophila* imaging experiments presented in this study, this was the fastest mode of IsoView single-color imaging, enabling four-view whole-animal volumetric functional imaging at 2 Hz.

Mode 2: simultaneous four-view imaging (phase-shifted confocal line detection). This mode takes advantage of the scheme of generating a scanned light sheet in which a thin laser beam is scanned vertically across each image plane, which makes it possible to acquire four views simultaneously by using a small scan phase delay in the vertical light-sheet sweeps between orthogonal illumination arms. As a result, the scanned laser beams in orthogonal arms are offset vertically throughout the light-sheet scans and do not cross paths at any time during the plane-illumination process. Additionally, light-sheet sweeps are synchronized with the respective sCMOS cameras' rolling shutters, in which a rolling band of camera pixel rows is exposed to fluorescence light simultaneously and read out. Thus the fluorescence light originating from each illuminated sample section is selectively imaged by confocal line detection on the respective cameras, and the phase delay in the propagation of rolling shutters in orthogonal cameras prevents cross-contamination of orthogonal views. For implementation of this mode, it is necessary that the rolling shutter direction and the light-sheet scan direction be matched. In all experiments presented here, the height of the confocal detection window was set to 72 pixels (29 μm), and the phase-shifted phase offset in orthogonal arms was set to 200 pixels (81 μm), which effectively eliminated cross-contamination with ballistic or scattered light even when imaging deep inside *Drosophila* embryos and larvae. Although the beam waist positions of the illuminating laser beams change continuously, an increase in the normalized s.d. of the light-sheet thickness across the field of view can be avoided by the use of light sheets with accordingly increased Rayleigh lengths and by initial positioning of all light sheet waists at the center of the specimen. For optimal image quality and physical coverage of the specimen, both light-sheet scan direction and rolling-shutter propagation direction are matched to the longer, lateral dimension of the specimen, minimizing the average penetration depth required for light-sheet illumination. This imaging mode

doi:10.1038/nmeth.3632

offers a combination of excellent background rejection and fast IsoView imaging speed, with the imaging speed dictated by the propagation speed of the rolling shutter in the sCMOS cameras and the sample size along the sample's longer, lateral dimension. For the current generation of sCMOS camera technology, the volumetric imaging rate in this imaging mode is slightly slower than in the first mode described above (1 Hz versus 2 Hz in our *Drosophila* experiments). Overall, the IsoView imaging mode described in this paragraph is the optimal choice for live imaging experiments that require maximum image quality and simultaneity of all four views.

Mode 3: two-color imaging. In this IsoView imaging mode, simultaneous four-view imaging is performed with light sheets at two different laser wavelengths along orthogonal arms. This imaging mode takes advantage of dual-band dichroic beam splitters that reflect illumination beams at two distinct wavelength ranges and transmit the corresponding fluorescence bands for detection. Additionally, only the fluorescence light for the corresponding channel is transmitted by each detection arm's band-pass filter, which eliminates fluorescence cross-contamination from light sheets propagating along the detection axes (and also blocks primary laser light from all four illumination arms). Thus, this mode utilizes the spectral separation of fluorescence light in orthogonal arms to perform simultaneous multicolor imaging. Similar to the sequential four-view imaging mode, this mode typically also uses the sCMOS cameras in rolling center mode, with the cameras oriented to perform rolling center wave propagation along the shorter, lateral dimension of the sample. For specimens expressing fluorescent double tags for the same structure or process of interest, this mode yields a complete four-view data set at twice the speed of the sequential-imaging mode, making it the fastest imaging mode. For imaging of fluorescent tags of two separate structures or processes in two distinct color channels, first a simultaneous four-view two-color volumetric data set is recorded using one wavelength configuration, and then a second, complementary simultaneous four-view two-color volumetric data set is acquired with the illumination wavelengths and the respective detection filters swapped between the orthogonal axes (**Supplementary Fig. 2**). Thus, in total eight image stacks are acquired in this mode, with four specimen views per color channel, with the same imaging speed as in the sequential-imaging mode described above. Lastly, we note that IsoView two-color imaging can also be performed in the relatively slower phase-shifted confocal line-detection mode discussed above, as long as the slightly reduced speed adequately samples the dynamic processes of interest. In this scenario, a simultaneous four-view volumetric recording using two color channels is followed by a second recording with the illumination wavelengths and the associated detection filters switched between orthogonal arms. Thus, eight image stacks, including four specimen views per color channel, are acquired at half the imaging speed of phase-shifted confocal line detection using a single color.

For the imaging experiments performed in this study, waists and Rayleigh lengths of light sheets were set to 6.3 ± 0.2 µm and 216 ± 20 µm (mean ± s.d., $n = 4$, corresponding to the microscope's four illumination arms), respectively, which corresponds to an effective illumination numerical aperture (NA) of 0.03 for 488 nm. A detailed overview of all experiment settings and imaging parameters for all experiments is provided in **Supplementary Table 2**.

To quantify the improvement in PSF isotropy with IsoView imaging and multiview deconvolution, we defined resolution anisotropy as the aspect ratio of the largest and the smallest PSF dimensions, minus 1 (the aspect ratio corresponding to perfect isotropy). Thus, resolution anisotropy A of a PSF with FWHM sizes S_x, S_y and S_z along x-, y- and z-axes, respectively, and FWHM sizes S_{d1} and S_{d2} along the diagonals of the y-z image plane (the dimensions of the theoretically worst performance in four-view deconvolved image data[16]) was calculated as follows:

$$A = \frac{\max(S_x, S_y, S_z, S_{d1}, S_{d2})}{\min(S_x, S_y, S_z, S_{d1}, S_{d2})} - 1 \quad (1)$$

We quantified signal-to-noise ratios for several imaging experiments by calculating the ratio F/N of the local fluorescence signal F, measured in gray levels above camera background, across the volume of randomly chosen cells expressing a nuclear marker (developmental imaging) or cytoplasmic GCaMP (functional imaging) and the s.d. N across a 50 × 50 pixel background region. Signal-to-noise ratios were then provided as the mean and s.d. across multiple such measurements of F/N.

IsoView multiview image registration. For specimens expressing fluorescent markers localized to cell nuclei (**Figs. 5** and **6**), we used Fiji's bead-based registration plug-in to facilitate multiview image registration[23]. In our IsoView functional-imaging data sets, however, suitable landmarks (somas with increased calcium levels relative to their neighbors and morphologies compatible with the registration algorithm) were too sparse for successful application of Fiji's registration method. We therefore developed a general two-step registration procedure capable of registering all specimen views simultaneously and robustly, independent of IsoView image content. This method is described below.

The view provided by the first camera is considered the reference view (although in principle any view can be set as the reference view). This view is not subjected to transformations, except for cubic interpolation along the detection axis to produce voxels with isotropic size.

In the first step of our registration procedure, we perform a coarse image alignment. After cubic interpolation for generating voxels with isotropic size, we embed all views in a common Cartesian coordinate system by flipping and/or transposing each view along one or several dimensions according to its initial orientation with respect to the reference view. Because each view corresponds to an optical detection axis that is rotated relative to the other view axes by a multiple of 90°, subsequent three-dimensional translation is sufficient to coarsely align the images. For this purpose, we temporarily downsample the image data by a factor of 4 and calculate the optimal translation vector using normalized cross-correlation (NCC) between each view and the reference view. Downsampling results in a substantial speed-up with no permanent effect on accuracy, as this initial coarse step is followed by a fine registration step.

In the second step of our registration procedure, we calculate affine transformations for all views simultaneously using a block-based matching scheme using RANSAC[28]. First, we detect a maximum of N_{max} points of interest in each volume by running local maxima suppression on the image data after difference of Gaussians (DoG) filtering. For each point of interest detected

in each image volume, we then search for possible matches in all other image volumes by extracting small blocks surrounding each point and looking for correspondences in the other views using NCC. As the images have already been coarsely aligned, we restrict this search to a small neighborhood to ensure efficiency as well as robustness. For each pair of views, we extract possible matches by using local maxima suppression on the NCC results and store a maximum of K matches per point of interest if they score above a predefined threshold. To find the correct affine transformation, we use RANSAC as follows. For each pair of views, we select four points of interest in one of the views uniformly and at random among all matched points. Because a three-dimensional affine transformation has 12 degrees of freedom, we require only four matches to determine the transformation between one pair of views. Within each of the four selected points, we randomly select a possible match among the K matches found before. Each possible match has a probability of being selected that is proportional to the NCC score of the match. Once all correspondences have been selected at random, we solve a linear system using least squares to simultaneously fit the affine transformations for all views. Finally, the affine transformations are tested on all matched points to count the number of inliers. This process is repeated M times, and the transformation with the largest fraction of inliers is kept as the final transformation. For the experiments presented in this study, typically between 100 and 300 inliers were found among all four views. The average residual error of the fit is 2–4 pixels.

For the data sets presented in this work, we used the following parameters: N_{max} equals 100, the sigma of the DoG filter is 6 pixels, and the block size is 144 × 144 × 144 pixels; the NCC threshold for considering possible matches for a given block is 0.8, K equals 3, and M equals 50,000.

IsoView multiview deconvolution. To enable rapid and efficient processing of the large amounts of multiview image data generated by each IsoView time-lapse recording (typically on the order of 10 TB per experiment), we wrote our own implementation of the Lucy-Richardson three-dimensional multiview deconvolution algorithm[4,17,24]. Our code is completely CUDA-based, which allows us to take full advantage of CUDA fast Fourier transform libraries and fast pixel-wise operations. Once the image data are loaded into the GPU, all iterations are executed entirely within the GPU, without the need for communication with the CPU, which minimizes data transfer between host workstation and GPU. Because typically not all specimen views can be loaded into the GPU memory at once, we split IsoView image data into blocks and process each block independently[24]. Our code thus takes full advantage of multi-GPU environments for parallel processing of multiple blocks. Overall, we found that our code was 22-fold faster than the fastest existing method[17] when we used a single GPU and 67-fold faster when we used a multi-GPU workstation equipped with four GPUs. These improvements allowed us to decrease the processing time for typical IsoView data sets on the order of 10 TB from several months to 2 d (considering overhead arising from disk input-output; **Supplementary Fig. 6b**). For the data sets presented in this study, multiview deconvolution was performed on two multi-GPU workstations, each equipped with four K20x Tesla GPUs and Intel Xeon E5-2689 CPUs with 2.7 GHz clock speed. A detailed quantitative analysis of the computation-time requirements of the IsoView multiview deconvolution software is provided in **Supplementary Figure 6b**.

Code availability. The open-source code and documentation for our IsoView deconvolution software are publically available at https://www.janelia.org/lab/keller-lab/software.

25. Chen, T.W. *et al.* Ultrasensitive fluorescent proteins for imaging neuronal activity. *Nature* **499**, 295–300 (2013).
26. Campbell, R.E. *et al.* A monomeric red fluorescent protein. *Proc. Natl. Acad. Sci. USA* **99**, 7877–7882 (2002).
27. Morin, X., Daneman, R., Zavortink, M. & Chia, W. A protein trap strategy to detect GFP-tagged proteins expressed from their endogenous loci in *Drosophila*. *Proc. Natl. Acad. Sci. USA* **98**, 15050–15055 (2001).
28. Fischler, M.A. & Bolles, R.C. Random sample consensus—a paradigm for model-fitting with applications to image-analysis and automated cartography. *Commun. ACM* **24**, 381–395 (1981).

doi:10.1038/nmeth.3632